Cation Size Variance Effects in Magnetoresistive Sr_2FeMoO_6 Double Perovskites

Falak Sher,[†,‡] A. Venimadhav,[§] Mark G. Blamire,[§] K. Kamenev,[‡] and J. Paul Attfield*[,‡]

Department of Chemistry, University of Cambridge, Lensfield Road, Cambridge CB2 1EW, Department of Materials Science and Metallurgy, University of Cambridge, Pembroke Street, Cambridge CB2 3QZ, and Centre for Science at Extreme Conditions, University of Edinburgh, King's Buildings, Mayfield Road, Edinburgh EH9 3JZ, U.K.

Received August 5, 2004. Revised Manuscript Received October 8, 2004

A series of $Sr_{2-x}(Ca_{0.55}Ba_{0.45})_xFeMoO_6$ ($0 \le x \le 0.8$) double perovskite oxides has been prepared to assess the effects of cation size variance, σ^2, at constant mean A site cation radius. All of the samples are ferromagnetic with Curie temperatures $T_C = 390-435$ K and show metal-to-insulator transitions at $T_{MI} = 10-115$ K. Both transition temperatures show a linear decrease with σ^2. The degree of Fe/Mo order increases with σ^2 from 81% to 90% under the synthesis conditions used, which increases the saturated magnetization and electronic conductivity of the ceramic samples. A decreasing structural anisotropy across the series accounts for a decrease in the magnetic coercivity. Negative colossal magnetoresistances (CMRs) are observed, up to 30% for the $x = 0.2$ sample at 5 K, but these show no trend with σ^2, which reflects the microstructural origin of the CMR in Sr_2FeMoO_6 materials.

Introduction

Materials exhibiting colossal magnetoresistance (CMR) undergo a large change in electrical resistance in response to an external magnetic field. A range of compounds have now been found to exhibit intrinsic CMR,[1,2] notably manganese oxide perovskites based on $LaMnO_3$. A CMR material should exhibit a highly spin polarized, semimetallic conductivity at the desired operating temperature (ideally room temperature (RT)) and so requires a ferro- or ferrimagnetic (FM) Curie temperature T_C well above RT. It is now well established that Curie temperatures of mixed-valence manganites cannot be increased above ~360 K by chemical substitution,[3] and materials with a substantially higher T_C are desirable. The recent discovery of RT magnetoresistance (MR) in Sr_2FeMoO_6 ($T_C \approx 440$ K) has stimulated research on this material and related double perovskite oxides.[4] Sr_2FeMoO_6 has a "rock salt" ordering of Fe and Mo atoms at alternating B sites of the ABO_3 perovskite structure, while Sr occupies the A sites. In a simple $Fe^{3+} + Mo^{5+}$ ionic description, the Fe^{3+} ($3d^5$, $S = 5/2$) ions are antiferromagnetically coupled to their Mo^{5+} ($4d^1$, $S = 1/2$) nearest neighbors, leading to an ideal saturation magnetization, $\mathbf{M}_S = 4\ \mu_B$/fu. However, a reduced saturation magnetization is commonly found due to antisite defects (occupancy of Fe sites by Mo and vice versa).[4−6] Band structure calculations[4] predict half-metallic behavior, where the electrons at the Fermi level are highly spin polarized, even at RT, making this phase very attractive for materials applications.

MR properties have been demonstrated in related double perovskites. Both Ca_2FeMoO_6 ($T_C \approx 377$ K)[7,8] and Ba_2FeMoO_6 ($T_C \approx 340$ K)[9] exhibit semimetallic and ferrimagnetic properties. Large low-field MR (LFMR) was also reported in the double perovskite $(Ba_{0.8}Sr_{0.2})_2FeMoO_6$ ($T_C \approx 345$ K).[10] However, the T_C values of these phases are modest compared to that of Sr_2FeMoO_6. A significant increase in T_C has been reported in the series $Sr_{2-x}La_xFeMoO_6$ (up to $T_C \approx 490$ K for $x = 1$), but this was accompanied by a strong increase of the Fe/Mo antisite disorder, which substantially decreased the magnetic moment and the LFMR.[11]

The substitution of Sr by La introduces both doping and disorder effects on the Fe−Mo oxide network. To discover the effect of the disorder in isolation, it is useful to study properties as a function of the A site cation size variance, $\sigma^2 = \langle r_A^2 \rangle - \langle r_A \rangle^2$ (r is the ionic radius, and the angular brackets denote an average). Size variance effects are known to be significant in a variety of perovskite-related oxides (CMR manganese perovskites,[3,12,13] doped La_2CuO_4 superconductors,[12−14] doped $BaTiO_3$ ferroelectrics[15]). To study the

* To whom correspondence should be addressed. E-mail: j.p.attfield@ed.ac.uk. Phone: +44 131 651 7229. Fax: +44 131 650 4743.
† Department of Chemistry, University of Cambridge.
‡ University of Edinburgh.
§ Department of Materials Science and Metallurgy, University of Cambridge.

(1) Ramirez, A. P. *J. Phys.: Condens. Matter* **1997**, *9*, 8171.
(2) Rao, C. N. R.; Raveau, B. *Colossal magnetoresistance and other related properties in 3d oxides*; World Scientific: Singapore, 1998.
(3) Rodriguez-Martinez, L. M.; Attfield, J. P. *Phys. Rev. B* **2000**, *63*, 024424.
(4) Kobayashi, K.-I.; Kimora, T.; Sawada, H.; Terakura, K.; Tokura, Y. *Nature* **1998**, *395*, 677.
(5) Ogale, A.; Ogale, S.; Ramesh, R.; Venkatesan, T. *Appl. Phys. Lett.* **1999**, *75*, 537.
(6) Balcells, Ll.; Navarro, J.; Bibes, M.; Roig, A.; Martinez, B.; Fontcuberta, J. *Appl. Phys. Lett.* **2001**, *78*, 781.
(7) Patterson, F. K.; Moeller, C. W.; Ward, R. *Inorg. Chem.* **1963**, *2*, 196.
(8) Galasso, F. *Structure, Properties and Preparation of Perovskite-type Compounds*; Pergamon Press: Oxford, 1969.
(9) Maignan, A.; Raveau, B.; Marti, C.; Hervieu, M. *J. Solid State Chem.* **1999**, *144*, 224.
(10) Kim, B. G.; Hor, Y. S.; Cheog, S. W. *Appl. Phys. Lett.* **2001**, *79*, 388.
(11) Navarro, J.; Frontera, C.; Balcells, Ll.; Martinez, B.; Fontcuberta, J. *Phys. Rev. B* **2001**, *64*, 092411.
(12) Attfield, J. P. *Int. J. Inorg. Mater.* **2001**, *3*, 1147.
(13) Attfield, J. P. *Cryst. Eng.* **2002**, *5*, 427.

10.1021/cm048711+ CCC: $30.25
Published on Web 12/07/2004

variance effect in a Sr perovskite without doping the material or changing the tolerance factor (equivalent to the average A site cation radius $\langle r_A \rangle$), a $Ca_{0.55}Ba_{0.45}$ mixture is used to replace Sr. These proportions are based on standard ionic radii,[16] 1.18, 1.31, and 1.47 Å for Ca, Sr, and Ba, respectively. Thus, the compositions $Sr_{2-x}(Ca_{0.55}Ba_{0.45})_xFeMoO_6$ ($x = 0$, 0.2, 0.4, 0.6, and 0.8) are equivalent to a σ^2 range from 0 to 0.009 Å^2 at constant mean A site cation radius $\langle r_A \rangle = 1.31$ Å.

Experimental Section

Polycrystalline samples of $Sr_{2-x}(Ca_{0.55}Ba_{0.45})_xFeMoO_6$ ($x = 0.0$, 0.2, 0.4, 0.6, and 0.8) were prepared by conventional solid-state reaction. Stoichiometric amounts of $SrCO_3$, $CaCO_3$, $BaCO_3$, Fe_2O_3, and MoO_3 were mixed, ground, pressed into pellets, and calcined at 1273 K for 10 h in air. The calcined mixtures were reground, pressed, and sintered at 1473 K for 14 h under flowing 5% H_2/95% Ar in a tube furnace. All the samples were heated again at 1273 K for 6 h in air and at 1473 K for 6 h in a 5% H_2/95% Ar atmosphere. Control of the oxygen partial pressure is crucial in the synthesis of Sr_2FeMoO_6 and related materials. Overreduction produces impurity phases such as $SrMoO_3$, Sr_2MoO_4, and Fe metal, whereas slightly oxidizing conditions lead to $SrMoO_4$ being produced along with the main phase. Initial attempts to prepare all the $Sr_{2-x}(Ca_{0.55}Ba_{0.45})_xFeMoO_6$ samples together under identical conditions were unsuccessful as it became evident that less reducing conditions were required for the higher x samples. Conditions were controlled by varying the flow rate of the 5% H_2/95% Ar mixture. Phase-pure samples of Sr_2FeMoO_6 were only obtained in the range of 60−75 cm^3/min gas flow rates, and this narrow window of gas flow rates shifts to slightly lower values with increasing x; for the $x = 0.8$ sample the upper limit for the gas flow rate was found to be 65 cm^3/min. Each sample was prepared individually using the above heating cycles and with appropriate 5% H_2/95% Ar flow rates. All of the samples were found to be >99% phase-pure by X-ray diffraction after this treatment except for the $x = 0.4$ material, for which the last two steps were repeated to eliminate traces of impurity phases.

Powder X-ray diffraction (XRD) profiles were recorded on a Bruker D8 Advance X-ray diffractometer (Cu Kα radiation, $\lambda = 1.5406$ Å) and were fitted using the program GSAS.[17] Magnetization measurements in the temperature range 20−470 K and fields up to 1 T were performed using a vibrating sample magnetometer (VSM). The resistivity (ρ) measurements, in zero and applied magnetic fields, were performed using a conventional dc four-probe arrangement in a Quantum Design physical properties measurement system (PPMS).

Results and Discussion

Crystal Structures. The crystal structure of Sr_2FeMoO_6 has been extensively studied using X-ray and neutron diffraction, and tetragonal *I*4/*mmm*,[18,19] *I*4/*m*,[20−22] or $P4_2/m$[23] has been proposed for the space group. *I*4/*m* permits rotation of the octahedra about the *z*-axis, which is not possible in *I*4/*mmm*, but these small oxygen displacements are difficult to detect in X-ray diffraction. Recently, Howard et al.[24] have suggested that the most probable space group is *I*4/*m*, and all of the present powder X-ray diffraction patterns were indexed and Rietveld-fitted using the tetragonal *I*4/*m* double perovskite model. However, we cannot critically distinguish between the I4/m and I4/mmm models using the present X-ray data. Figure 1 shows the XRD pattern of the $x = 0.4$ sample as an example. Rietveld fits were used to refine the unit cell parameters and the Fe/Mo occupancies of the B and B′ sites in the $A_2BB'O_6$ double perovskite structure. All of the samples showed sharp diffraction peaks with no appreciable particle size broadenings (the Lorentzian particle size broadening term refined to zero). A small strain broadening was observed, and this was fitted by varying the Lorentzian strain parameter (LY in the GSAS program) while the Gaussian width (GW) was fixed at an average value. The refinement results are given in Table 1, and bond lengths and angles are given in Table 2.

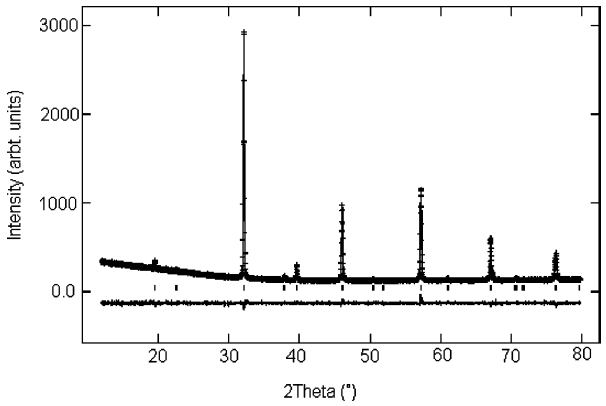

Figure 1. Rietveld fit to powder X-ray diffraction data for $Sr_{1.6}Ca_{0.22}Ba_{0.18}FeMoO_6$ indexed on a tetragonal *I*4/*m* unit cell. Observed (plus signs) and calculated (solid line) intensities are shown, with the difference below.

The *a* and *c* lattice parameters, and hence the unit cell volume, increase slightly with σ^2. This is expected because volume scales as $\langle r_A^3 \rangle$; although the mean A site cation radius $\langle r_A \rangle$ is constant, $\langle r_A^n \rangle$ increases for $n > 1$ as the variance σ^2 increases. The $c/(\sqrt{2})a$ ratios in Table 1 increase with σ^2, showing that the tetragonal lattice distortion is decreasing. The increase in Lorentzian strain broadening (LY) down the series is thus a reflection of the increasing A site cation size fluctuations rather than the decreasing tetragonality.

A high degree of Fe/Mo ordering is observed in all samples, and counterintuitively, this shows an increase from 81% to 90% with an increase of the A site cation size variance σ^2. As shown in Table 2, the mean ⟨Fe−O⟩ (B site) bond length increases while that of ⟨Mo−O⟩ (B′ site)

(14) Attfield, J. P.; Kharlanov, A. L.; McAllister, J. A. *Nature* **1998**, *394*, 157.
(15) Sinclair, D. C.; Attfield, J. P. *Chem. Commun.* **1999**, *16*, 1497.
(16) Shanon, D. *Acta Crystallogr.* **1976**, *32*, 751.
(17) Larson, A. C.; von Dreele, R. B. *GSAS: General Structure Analysis System*; LANSCE, MS-H805; Los Alamos National Laboratory: Los Alamos, NM, 1994.
(18) Tomioka, Y.; Okuda, T.; Okimoto, Y.; Kumai, R.; Kobayashi, K.-I.; Tokura, Y. *Phys. Rev. B* **2000**, *61*, 422.
(19) Moritomo, Y.; Zhu, S.; Machida, A.; Akimoto, T.; Nishibori, E.; Takata, M.; Sakata, M.; Ohoyama, K. *J. Phys. Soc. Jpn.* **2000**, *69*, 1723.
(20) Chmaissem, O.; Kruk, R.; Dabrowski, B.; Brown, D. E.; Xiong, X.; Kolesnik, S.; Jorgensen, J. D.; Kimball, C. W. *Phys. Rev. B* **2000**, *62*, 14197.
(21) Sanchez, D.; Alonso, J. A.; Garcia-Hernandez, M.; Martinez-Lope, M. J.; Martinez, L. *Phys. Rev. B* **2002**, *65*, 104426.
(22) Nakamura, S.; Oikawa, K. *J. Phys. Soc. Jpn.* **2003**, *72*, 3123.
(23) Ritter, C.; Ibarra, M. R.; Morellon, L.; Blasco, J.; Garcia, J.; De Teresa, J. M. *J. Phys.: Condens. Matter* **2000**, *12*, 8295.
(24) Howard, C. J.; Kennedy, B. J.; Woodward, P. M. *Acta Crystallogr., B* **2003**, *59*, 463.

Table 1. Unit Cell Parameters, Fe/Mo Order, Saturated Magnetization, and Transition Temperatures for the $Sr_{2-x}(Ca_{0.55}Ba_{0.45})_xFeMoO_6$ Samples

x	σ^2 (Å^2)	a (Å)	c (Å)	c/(√2)a	LY (×0.01°)	Fe/Mo order (%)	$\mathbf{M}_S$ (μ_B/fu)	T_C (K)	T_{MI} (K)
0.0	0	5.5806(1)	7.8761(3)	0.9980	12.42(6)	81.2(3)	2.86	435	85
0.2	0.0022	5.58556(9)	7.8823(2)	0.9979	14.17(7)	88.8(4)	3.50	425	115
0.4	0.0044	5.58342(8)	7.8816(2)	0.9982	15.14(7)	89.9(4)	3.72	430	55
0.6	0.0066	5.5927(2)	7.8988(4)	0.9987	16.62(9)	90.4(5)	3.63	402	30
0.8	0.0088	5.5950(1)	7.9029(3)	0.9988	16.15(8)	89.2(5)	3.64	389	10

Table 2. Selected Bond Lengths and Bond Angles for the $Sr_{2-x}(Ca_{0.55}Ba_{0.45})_xFeMoO_6$ Samples

bond length (Å)/ bond angle (deg)	$x = 0$	$x = 0.2$	$x = 0.4$	$x = 0.6$	$x = 0.8$
A[a]−O (1) × 4	2.7879(2)	2.7894(6)	2.7910(3)	2.7977(9)	2.7981(9)
A−O (2) × 4	2.650(3)	2.644(4)	2.631(3)	2.632(4)	2.596(4)
A−O (2) × 4	2.940(4)	2.954(4)	2.968(4)	2.976(5)	3.019(4)
⟨A−O⟩	2.793(3)	2.796(3)	2.797(3)	2.802(4)	2.804(3)
Fe−O(1) × 2	2.033(7)	2.034(7)	2.031(2)	2.053(2)	2.072(3)
Fe−O(2) × 4	2.011(1)	2.027(4)	2.042(8)	2.074(3)	2.083(1)
⟨Fe−O⟩	2.022(4)	2.030(5)	2.036(7)	2.064(3)	2.078(2)
Mo−O(1) × 2	1.931(7)	1.925(7)	1.923(2)	1.886(3)	1.888(3)
Mo−O(2) × 4	1.941(1)	1.937(1)	1.933(8)	1.932(1)	1.917(1)
⟨Mo−O⟩	1.936(4)	1.931(4)	1.928(7)	1.909(2)	1.902(2)
Fe−O(1)−Mo (deg)	180	180	180	180	180
Fe−O(2)−Mo (deg)	168.08(3)	167.77(3)	166.18(3)	165.9(4)	162.72(3)

[a] A = Ca, Sr, and Ba.

decreases with σ^2. This is partly an artifact of the increasing Fe/Mo site order, as the crystallographic distances average over the Fe/Mo order at the B and B′ sites. However, the magnitude of the effect shows that an electronic (valence transfer) contribution is also present. This can be explained in terms of the larger ionic radius of Fe^{2+} (0.78 Å) compared to Fe^{3+} (0.645 Å) and smaller ionic radius of Mo^{6+} (0.59 Å) compared to Mo^{5+} (0.61 Å). As the charge difference between Fe^{2+} and Mo^{6+} is larger than between Fe^{3+} and Mo^{5+}, the increased order favors the former charge states. Hence, the observed trend in distances is consistent with the increase in Fe/Mo ordering. A high Fe/Mo order is also observed in small $\langle r_A \rangle$ materials such as Ca_2FeMoO_6.[25] It has been reported[6] that B site ordering in Sr_2FeMoO_6 is thermodynamically controlled at temperatures comparable to the synthesis temperature (1473 K), so the observed increase in B site order is likely to be an equilibrium thermodynamic effect rather than an artifact of the reaction kinetics. σ^2-induced ordering of orbital (Jahn−Teller) distortions in doped $AMnO_3$ perovskites has previously been reported, so it is evident that an increase in the A site cation disorder can induce or improve long-range ordering phenomena associated with the BO_3 network in ABO_3 perovskites.[3]

Magnetization Measurements. Magnetization versus temperature ($\mathbf{M}-T$) plots of the $Sr_{2-x}(Ca_{0.55}Ba_{0.45})_xFeMoO_6$ ($0 \le x \le 0.8$) samples are shown in Figure 2. All the samples show a paramagnetic to ferromagnetic transition.The Curie temperatures, T_C, of the samples were estimated by extrapolating the maximum ($-d\mathbf{M}/dT$) slope to zero magnetization. The plot of T_C against σ^2 shown in Figure 3 reveals a strong negative linear correlation for four of the five samples. However, the $x = 0.4$ sample does not fit this trend, which may be a consequence of the additional heating cycle used during the synthesis of this sample, as described above. The long-range Fe/Mo ordering parameter for this sample (Table 1) is not anomalous, but the short-range clustering of antisite defects may be changed by the additional heating cycle, giving the unexpectedly high T_C. This is corroborated by the higher saturated magnetization for this sample (Table 1).

Magnetization isotherms at 20 K (Figure 4) are typical of soft ferromagnetic oxides, with very small remanences and coercivities. The saturation magnetizations, $\mathbf{M}_S$, lie below the theoretical value of 4 μ_B per formula for fully ordered A_2FeMoO_6 double perovskites. This reduction is principally a consequence of Fe/Mo antisite disorder,[5,6,11] and the overall increase in $\mathbf{M}_S$ with σ^2 (Table 1) correlates with the increase in Fe/Mo order.

Figure 5 shows the variation of coercivity, $\mathbf{H}_C$, with σ^2 derived from the 20 K hysteresis loops in Figure 4. The observed decrease in $\mathbf{H}_C$ (an increasing magnetic softness

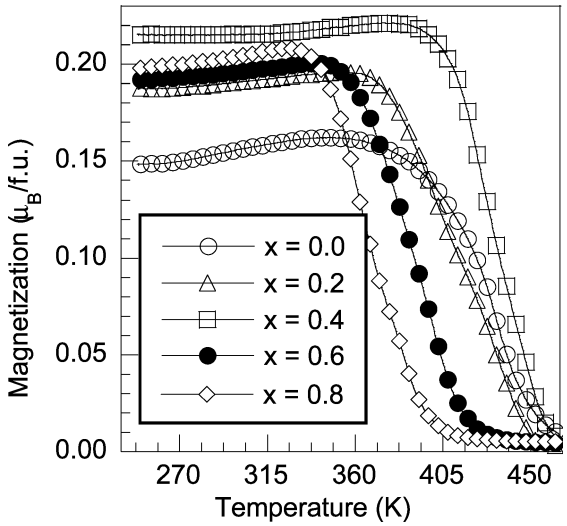

Figure 2. Magnetization measurements for $Sr_{2-x}(Ca_{0.55}Ba_{0.45})_xFeMoO_6$ ($0 \le x \le 0.8$) samples in a 100 Oe applied field.

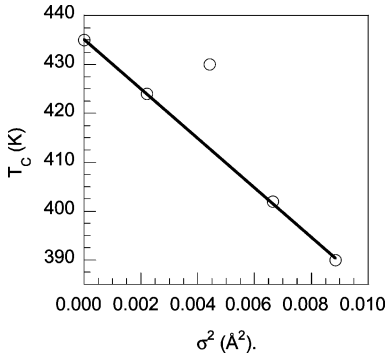

Figure 3. Variation of the Curie temperature, T_C, with σ^2 (Å^2) in the $Sr_{2-x}(Ca_{0.55}Ba_{0.45})_xFeMoO_6$ series, showing a linear fit to the data (excluding the $x = 0.4$ sample).

(25) Chan, T. S.; Liu, R. S.; Guo, G. Y.; Hu, S. F.; Lin, J. G.; Chen, J. M.; Attfield, J. P. *Chem. Mater*. **2003**, *15*, 425.

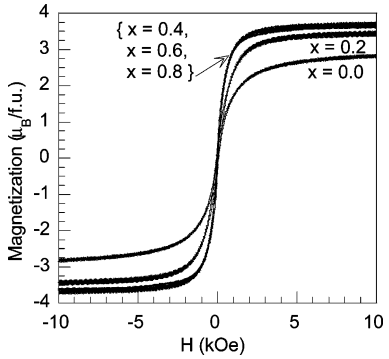

Figure 4. Magnetization field loops at 20 K for the $Sr_{2-x}(Ca_{0.55}Ba_{0.45})_xFeMoO_6$ ($0 \le x \le 0.8$) samples. The $x = 0.4-0.8$ data are essentially identical.

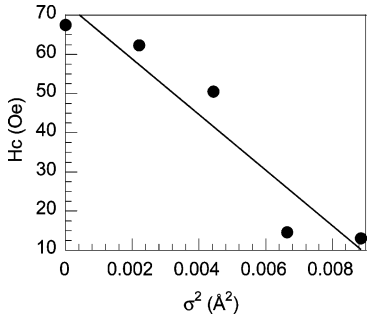

Figure 5. Variation of the 20 K coercivity, $\mathbf{H}_C$, with σ^2 in the $Sr_{2-x}(Ca_{0.55}Ba_{0.45})_xFeMoO_6$ series.

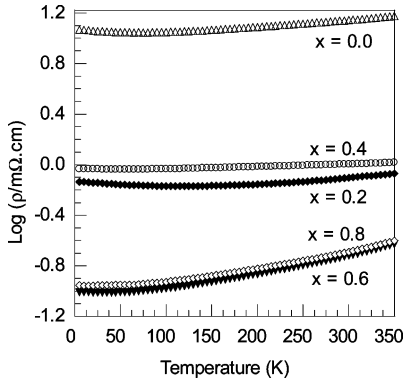

Figure 6. Resistivities of $Sr_{2-x}(Ca_{0.55}Ba_{0.45})_xFeMoO_6$ ($0 \le x \le 0.8$) ceramic pellets.

with σ^2) suggests that the structures are becoming more structurally isotropic. This is consistent with the decrease in the tetragonal distortion observed in the $c/(\sqrt{2})a$ cell parameter ratios in Table 1.

Electronic Transport Properties. The temperature variations of the resistivities (ρ) of ceramic pellets of the $Sr_{2-x}(Ca_{0.55}Ba_{0.45})_xFeMoO_6$ ($0 \le x \le 0.8$) samples are shown in Figure 6. The sample resistivities of $10^{-4}-10^{-2}$ Ω·cm approach the $\sim 10^{-2}$ Ω·cm (minimum metallic conductivity) limit typical of metallic oxides having significant disorder. The semimetallic behavior of Sr_2FeMoO_6 results from the ferrimagnetic spin ordering coupled with the $Fe^{2+} + Mo^{6+} \leftrightarrow Fe^{3+} + Mo^{5+}$ valence degeneracy first proposed by Sleight and Weiher.[26] This is supported by recent band structure calculations,[4] which show that the Fermi level lies within a narrow conduction band made from Mo 4d and Fe 3d down-spin t_{2g} and O 2p states.

(26) Sleight, A. W.; Weiher, J. F. *J. Phys. Chem. Solids* **1972**, *33*, 679.

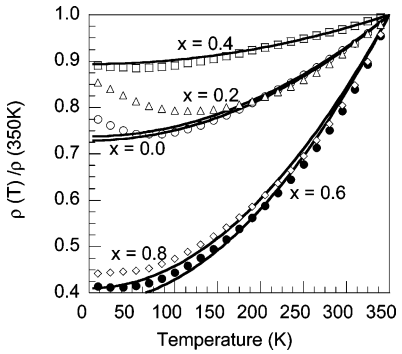

Figure 7. Normalized resistivities ($\rho(T)/\rho(350$ K)) for the $Sr_{2-x}(Ca_{0.55}Ba_{0.45})_xFeMoO_6$ samples showing fits of $p + qT^2$ (solid lines) dependence.

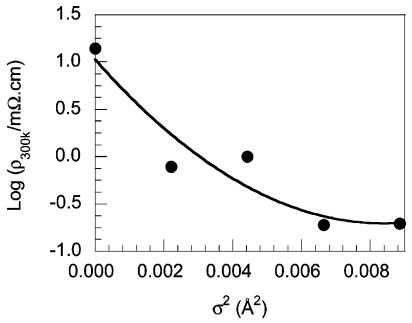

Figure 8. Variation of the 300 K resistivity (on a log scale) with σ^2.

The sample resistivities show an irregular decrease with x and σ^2 (300 K values are shown in Figure 8). The irregularities are likely to result from small sample-to-sample differences in packing density and intergrain contacts. A similar kind of dependence of the sample resistivities on the grain size has also been reported for $A_{(2-x)}A'_xFeMoO_6$ (A = Sr, Ca, or Ba, and A′ = La)[27] and $(Ba_{0.8}Sr_{0.2})_{2-x}La_xFeMoO_6$.[28] The dominant intrinsic contribution is likely to be the increased Fe/Mo order (Table 1) induced by the increasing size variance σ^2. Fe/Mo antisite defects disrupt the local magnetic order and so strongly modify the local electronic structure. This evidently outweighs the intrinsic effect of the cation size disorder, which is to create local Fe−O−Mo bond angle variations that act as a disorder potential and increase the resistivity with σ^2.

At high temperatures (>200 K), the resistivities follow a T^2 dependence that is typical of electron−electron scattering in correlated metallic conductors,[19] as shown in Figure 7. On cooling to lower temperatures, the effects of disorder scattering become dominant, and this ultimately leads to a metal ($d\rho/dT > 0$) to insulator (or semiconductor, $d\rho/dT < 0$) transition marked by a minimum in the resistivity at T_{MI}.

The ordering temperatures for many electronic transitions have a negative linear correlation with σ^2. The slope of the linear fit to T_C in Figure 3 gives a value of $-dT_C/d\sigma^2 = 5200$ K Å^{-2} and $-dT_{MI}/d\sigma^2 = 10500$ K Å^{-2} from Figure 9. These are comparable to the values of 10000−20000 K Å^{-2} found for the simultaneous Curie and metal−insulator transitions in ferromagnetic manganites,[3] and to $-dT_c/d\sigma^2 = 3000-7000$ K Å^{-2} for the superconducting critical

(27) García-Hernández, M.; Martínez, J. L.; Martínez-Lope, M. J.; Casais, M. T.; Alonso, J. A. *Phys. Rev. Lett.* **2001**, *86*, 2443.
(28) Serrate, D.; De Teresa, J. M.; Blasco, J.; Ibarra, M. R.; Morellon, L.; Ritter, C. *Appl. Phys. Lett.* **2002**, *80*, 4573.

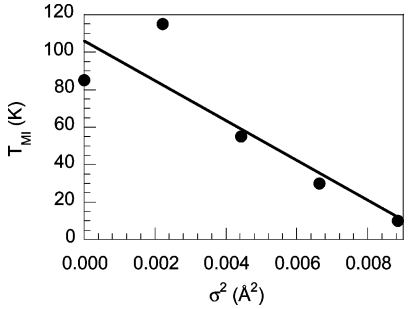

Figure 9. Variation of the metal-to-insulator transition temperature, T_{MI}, with σ^2 for $Sr_{2-x}(Ca_{0.55}Ba_{0.45})_xFeMoO_6$ samples with a linear fit.

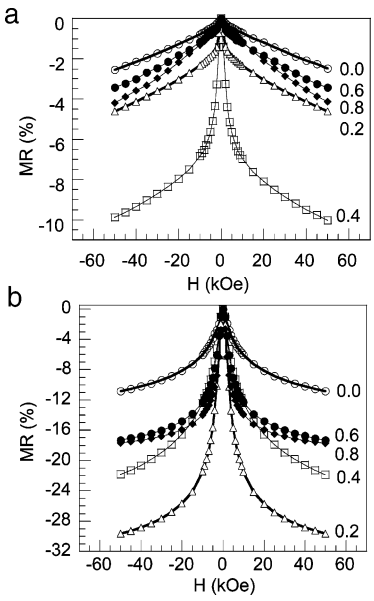

Figure 10. MR for the $Sr_{2-x}(Ca_{0.55}Ba_{0.45})_xFeMoO_6$ ($0 \le x \le 0.8$) ceramic pellets as a function of field with x values at (a) 300 K and (b) 5 K.

temperatures T_c of doped La_2CuO_4 superconductors. Hence, Sr_2FeMoO_6 displays the generic strong sensitivity of electronic transition temperatures to lattice disorder in perovskite oxides. This is the first demonstration of the effect in the double perovskite systems, as the practical difficulties of preparing series of samples under identical conditions make such studies more demanding than for simple perovskites.

Field-dependent MR data of the samples at 300 and 5 K are shown in Figure 10. A large negative low-field MR is observed in these ceramic samples, as magnetotransport is limited by spin-dependent scattering at grain or magnetic domain boundaries.[4] The boundaries result in a tunneling MR, as the hopping of spin-polarized electrons between magnetic domains is critically affected by their relative magnetization directions, and hence may be controlled by an external magnetic field via the domain rotation process. The crossovers between the steep, low-field, and the more gradual, high-field, MR processes in Figure 10 coincide with the onset of the magnetization plateaus at ~2 kOe in the **M**−**H** plots (Figure 4). The high-field (>20 kOe) increases in MR show the intrinsic decrease of spin-dependent scattering with field. There is a linear correlation among the Fe/Mo ordering, saturation magnetization, $\mathbf{M}_S$, and low-field MR effect as reported elsewhere.[27]

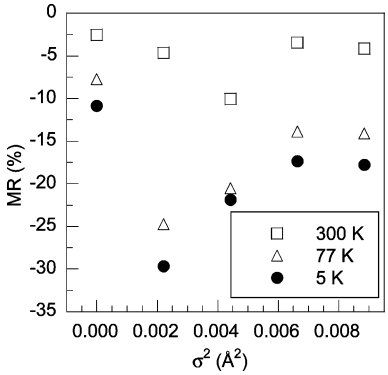

Figure 11. MR at 5 T shown as a function of σ^2 at 5, 77, and 300 K.

Figure 11 shows the variation of the 50 kOe MR with σ^2 at 5, 77, and 300 K. No trends are evident; the largest −MR value is 10% in the $x = 0.4$ sample at 300 K, but at lower temperatures the $x = 0.2$ sample shows the largest effect up to 30% at 5 K. This demonstrates that the MR in Sr_2FeMoO_6-type materials is dependent mainly upon the microstructure of grains and magnetic domains, which are more sensitive to small variations in sample preparation conditions than to structural changes such as the effect of σ^2.

Conclusions

This study of ceramic $Sr_{2-x}(Ca_{0.55}Ba_{0.45})_xFeMoO_6$ ($0 \le x \le 0.8$) materials enables the effects of cation size variance σ^2 on various properties of the ferromagnetic Sr_2FeMoO_6 double perovskite to be assessed. Intrinsic trends are observed despite variation of the preparation conditions with x, but the thermal history (in particular of the repeatedly annealed $x = 0.4$ sample) can cause further variations of the properties. The generic linear reduction of electronic transition temperatures with σ^2, previously seen in other perovskite-related oxides (manganites and cuprates), is nevertheless found for the Curie and the metal−insulator transitions in Sr_2FeMoO_6. The main structural influence of σ^2 under these synthesis conditions is to increase the degree of Fe/Mo ordering at the B sites. This increases the saturated magnetization and the conductivity of the samples. A decreasing structural anisotropy across the series accounts for a decrease in the magnetic coercivity. Large negative magnetoresistances are observed, up to 30% for the $x = 0.2$ sample at 5 K, but these show no trend with σ^2. This emphasizes the microstructural origin of the CMR in these materials; small sample-to-sample differences in the connectivity of grains or magnetic domains are more significant than the underlying change in A site cation disorder.

Acknowledgment. We thank the Ministry of Science and Technology, Government of Pakistan, and EPSRC (Grant GR/R30518) for funding.

CM048711+